Three-dimensional Printed Polylactic Acid and Hydroxyapatite Composite Scaffold with Urine-derived Stem Cells Treatment for Bone Defects

Xiang Zhang
Sichuan University West China Hospital
Jialei Chen
Sichuan University West China Hospital
Hongren Wang
Sichuan University West China Hospital
Xin Duan (xinduan_su@163.com)
Sichuan University West China Hospital https://orcid.org/0000-0003-1685-1021
Feng Gao
Sichuan University West China Hospital

Research article

Keywords: Urine-derived stem cells, Skull defects, 3D printing, Bone regeneration, Tissue engineering

Posted Date: November 1st, 2021

DOI: https://doi.org/10.21203/rs.3.rs-996295/v1

Abstract

BACKGROUND: Bone defects still pose various challenges in osteology. As one of the treatment options for bone defects, bone tissue engineering requires biomaterials with good biocompatibility and seed cells with good differentiation capacity. This study aimed to fabricate a 3D-printed polylactic acid and hydroxyapatite (PLA/HA) composite scaffold with urine-derived stem cells (USCs) to study its therapeutic effect in a model of skull defect in rats.

METHODS: USCs, isolated and extracted from the urine of healthy adult males, were inoculated onto a 3D-printed PLA/HA composite scaffold and a PLA scaffold. Skull defect model rats were randomly divided into three groups (control, PLA, and PLA/HA). Twelve weeks after implanting scaffolds containing USCs into rats with a skull defect, the therapeutic efficacy was evaluated by real-time PCR, micro-CT, histology, and immunohistochemistry.

RESULTS: The 3D-printed PLA/HA composite scaffold had good mechanical properties and porosity. The adhesion and proliferation of USCs on scaffolds also demonstrated excellent biocompatibility. PLA and PLA/HA containing USCs promoted bone regeneration in the defect area, supported by the general observation and CT images at 12 weeks after treatment, with coverage of 74.6%±1.9% and 96.7%±1.6%, respectively. Immunohistochemical staining showed a progressive process of new bone formation on PLA/HA scaffolds containing USCs at the defect site compared to that in PLA and control groups.

CONCLUSION: The 3D-printed PLA/HA composite scaffold with USCs was successfully applied to the skull defect in rats. Under the linkage of the scaffold, the proliferation, differentiation, and osteogenesis expression of USCs were promoted near the bone defect area. These findings demonstrated broad application prospects of PLA/HA scaffolds with USCs in bone tissue engineering.

Introduction

Bone defects are common in clinical practice and caused by different factors. Millions of bone transplants are performed each year. Therefore, bone defect repair has always been the focus of research and attention in orthopedics[1]. Traditional treatments for bone defects include autogenous bone grafts, allografts, and bone graft substitutes. With the assistance of osteoblasts, extracellular matrix, and bioactive factors, the transplanted bone tissue performs its function of fracture healing and enhances the mechanical stress at the defect site. However, the traditional treatment for bone defects has apparent limitations due to immune rejection, risk of disease transmission, poor bone histocompatibility, and other problems [2]. Faced with the increasing need for better treatment of bone defects, the emergence of tissue engineering and 3D printing technology gives us a new method and direction [3].

Tissue engineering combines suitable scaffolds with seed cells proliferated *in vitro* to repair the bone defect via the biomimetic method [4]. In recent years, it has been found that seed cells such as bone marrow stromal cells, adipo-derived stromal cells, and mesenchymal stem cells (MSCs) have the capacity of multidirectional differentiation [5, 6]. Tissue grafts produced by seed cells perform better than artificial

materials, providing a feasible way to enable bone regeneration. Induced pluripotent stem cells are highly differentiated, but limited sampling sites, insufficient donors, and ill-equipped cell homing prevent them from clinical application. In particular, the underlying carcinogenicity of seed cells makes their clinical efficacy uncertain.

Urine-derived stem cells (USCs) are pluripotent adult stem cells whose biological properties resemble MSCs. USCs play a crucial role in promoting tissue regeneration and regulating immunity by secreting various cytokines [7]. Compared with other seed cells, USCs have the potential to differentiate between bone, cartilage, and fat, and have the advantages of being easy to obtain, free from trauma, and strong practicability [8–10]. Currently, USCs have shown sound therapeutic effects in animal models of urinary system, nerve tissue, and skeletal muscle tissue injury. As seed cells, they are also used for urinary system reconstruction and bone tissue engineering [11–14]. Therefore, a therapeutic strategy based on USCs has a bright prospect for bone defect repair.

When applied to medical research, 3D printing technology has the advantages of short production cycles and low processing costs. With the help of computer-aided design (CAD), desirable engineered bone scaffolds are easy to acquire, which solves the problem of preparing scaffolds with unique structures and distribution patterns [15]. Compared with traditional technology, 3D printing may control the structure of biological scaffolds from the macro to the microscale, producing different types of tissue engineering scaffolds and achieving precision medicine [16]. As a standard-used technology in 3D printing, fused-deposition modeling (FDM) technology demands less equipment, more straightforward operation, and lower price. By making the raw materials into filament-like fixed and melting the filament-like materials through the nozzle heating, the target bracket can be printed on the operating plate [17, 18].

Selecting a suitable scaffold is an essential step in bone tissue engineering. Due to its biocompatibility and degradability, polylactic acid (PLA), one of the commonly used synthetic polyester materials for preparing scaffolds, meets the requirements of bone tissue engineering. However, the degradation of polylactic acid under normal physiological conditions can generate acidic substances and cause inflammation [19]. Zhang et al. found that the preparation of composite scaffolds by adding hydroxyapatite (HA) into PLA scaffolds can reduce the inflammatory reaction of PLA scaffolds and increase their mechanical strength and bone induction ability [20, 21]. Previous studies have demonstrated the mechanical properties of PLA enhanced with HA, and the applicability of PLA/HA scaffolds in tissue engineering [22]. However, such a good tolerance scaffold has not been applied to the development of USCs for bone regeneration, and their performance in tissue engineering has not been assessed.

Thus, we prepared a 3D-printed PLA/HA composite scaffold seeded with USCs isolated from adult healthy male urine. Then, we investigated its feasibility for bone defect repair based on the results of osteogenic induction in a rat skull defect model.

Materials And Methods

Isolation and cultivation of USCs

The age and health status of the urine providers are important for the extraction of USCs [23]. This study collected urine from young volunteers aged 20–30 years from the Physical Examination Center of West China Hospital of Sichuan University. The clean urine was put into a centrifuge tube containing 1 ml 1% penicillin–streptomycin, then centrifuged at 1500 rpm for 15 min. The bottom 5 ml of urine was flushed with phosphate-buffered saline (PBS) and centrifuged at 1500 rpm for 5 min. The collected cell precipitates were added to six-well plates, with 2 ml DMEM supplemented with 2% (vol/vol) fetal bovine serum (FBS), 10 ng/ml human epidermal growth factor (hEGF), 2 ng/ml platelet-derived growth factor (PDGF), 1 ng/ml transforming growth factor-β (TGF-β), 0.5 μM cortisol (hydrocortisone), 25 μg/ml insulin, 20 μg/ml transferrin, 549 ng/ml adrenaline, L-glu and antibiotics. DMEM in each plate was replaced every 3 days. Subsequently, they were incubated at 37℃ and 5% CO_2 for further experiments. After the fusion rate of primary cells reached 80–90%, the cell pellets were flushed with PBS, then, prepared trypsin solution was added to digest the adherent cells. After centrifugation at 1500 rpm for 5 min, cell pellets were subcultured in a 25T breathable culture flask with a CO_2 concentration of 5% at 37℃. Cells were frozen and kept in liquid nitrogen after the subculture reached the fourth generation. The fourth generation of USCs was used for our experiments.

Identification of USCs

It is generally believed that USCs express the surface antigens of MSCs (CD29, CD44, CD54, CD73, CD90, and CD105) rather than hematopoietic stem cell markers (CD11b, CD14, CD19, CD31, CD34, CD45, and HLA-DR) [7, 9]. USCs were identified by flow cytometry. First, the cell concentration of the fourth-generation USCs was adjusted to 1×10^7 cells/200 μl. Then, high expression of CD73, CD90, and CD105 on the stem cell surface was used as USC-positive indicators, while low expression of CD34, CD45, MHCII, HLA-DR, and other stem cell surface antigens were used as USC-negative indicators. After adding the corresponding antibodies, USCs were incubated at 4℃ for 30 min. Finally, they were flushed with PBS repeatedly and identified by flow cytometry.

Multidirectional differentiation of USCs

It has been reported that USCs can differentiate into adipoblasts, osteoblasts, and chondroblasts under the appropriate environment and induction medium [7, 24]. The osteogenic differentiation ability of USCs was identified by alizarin red staining and verified by alkaline phosphatase staining. Alizarin red staining showed that the reaction of cell calcium depositions was positive. Under alkaline conditions, alkaline phosphatase can hydrolyze naphthol phosphate AS-Mx to produce naphthol, which can be captured by diazonium salts, resulting in the colored insoluble precipitate. USCs were cultured in an osteogenic medium for 3 weeks. After being fixed with 4% paraformaldehyde for 30 min, the cell slides were stained with Alizarin red dye in an incubator at 37℃ for 30 min. The prepared samples were observed by microscopy. Besides, adipogenic and chondrogenic differentiation of USCs was identified by oil red O lipid staining and Alcian blue staining.

Preparation of 3D printed PLA/HA composite scaffold

PLA and HA (Sigma–Aldrich, America) were weighed according to different mass ratios (9:1). PLA was dissolved in trichloromethane, which was heated to 60℃ in a water bath. During the stirring process, HA powder was added and blended well until all ingredients were fully dissolved. After sonication in an ultrasonic oscillator for 15 min, PLA and HA were thoroughly stirred for 10 h under an electromagnetic agitator to ensure that HA was evenly dispersed in the PLA, as previously described [25]. After the drying process, the mixed ingredients were added to the 3D wire-forming machine to make a solid wire with a diameter of 5 mm. CAD software was used to design the shape of the bracket (rectangular sheet with a length and width of 20 mm and thickness of 1.5 mm), and the porosity was determined at nearly 65%, as described previously [26].

Scanning electron microscopy (SEM) analysis, energy-dispersive X-ray spectroscopy (EDS), and mechanical property analysis

The general view of the 3D-printed PLA and PLA/HA composite scaffolds was observed, and their sizes were measured. The microscopic morphology of the 3D-printed PLA and PLA/HA composite scaffolds was observed through SEM (JSM-IT300HR, Shimadzu, Japan). EDS was used to determine the presence of HA in PLA/HA. A universal mechanical properties tester (Shimadzu; n = 5 in each group) was used to measure the mechanical tensile strain of these two scaffolds (all samples were continuously exposed to a constant strain rate of 0.5 mm/min without preloading until the maximum deformation was achieved).

Porosity and in vitro degradation rates of scaffolds

The porosity of the material (M) was measured by the soaking method. We calculated the volume (V) and weighed the mass (M0) of the scaffold. The sample was immersed in absolute alcohol for 24 h, and the pores of the scaffold were filled under pressure. Samples were taken out and weighed (M1). The porosity of each scaffold was calculated as follows: M (%) = (M1−M0)/V·100% (M represents the porosity of each scaffold; M0 represents the initial weight of the scaffold; M1 represents the weight of scaffolds after being immersed; V represents the volume of the scaffold).

The general calculation for the degradation rates of scaffolds was completed in PBS (pH 7.4), which was named the weight loss method [27]. After being dried and weighed (W0), PLA and PLA/HA scaffolds (n=4 in each group) were put into the configured PBS, which was replaced every week, and heated in a water bath at 37℃. At each time point (1–8 weeks), samples were collected, dried, and weighed (W1). The degradation rate of the material was calculated as follows: W_T (%) =(W_0W_1)/W_0·100% (W_T represents the degradation rate of the scaffold; W_0 represents the initial weight of the scaffold; W_1 represents the weight of the scaffold after drying).

Viability and proliferation of USCs on scaffolds

The fourth-generation USCs were carefully seeded on PLA and PLA/HA composite scaffolds (cell concentration: 10^5 /ml, n = 4 of each type). After being cultured in DMEM high glucose for 3 days, they were flushed and fixed with 2.5% glutaraldehyde. The scaffolds with USCs were stored in a vacuum freeze-dryer for 24 h. Then, they went through a process of metal spraying. All the samples were evaluated under SEM for morphology and adhesion of cells. Cell permeabilization was finished on scaffolds with the action of 0.5% TritonX-100 solution. TRITC phalloidin (200 μl) was added to the surface of the scaffolds. The scaffolds were incubated for 30 min in a dark room. DAPI solution (200 μl) was added to the surface of the scaffolds to complete the process of nuclear counterstain after a PBS rinse. The cytoskeleton was observed by confocal laser scanning microscopy and immunofluorescent staining technique [TRITC excited/emitter filters (Ex/EM=540/570 nm) and DAPI excited/emitter filters (Ex/EM=364/454 nm)]. A CCK-8 Kit was used to proliferate USCs under scaffolds leach liquor, which was acquired by using DMEM to immerse the scaffolds for 24 h in a 37°C incubator. USCs were seeded in 96-well plates and incubated for 24 h, then leaching liquor supplemented with 10% FBS and 1% penicillin/streptomycin was used for the cell culture medium. At different time points (1, 3, 5, and 7 days after the experiment), CCK-8 reagent and a full-wavelength microplate reader were used to measure the absorbance of the soaking solution at 450 nm in different groups.

Quantitative RT-PCR analysis of osteogenic gene expression

The fourth-generation USCs were added into osteogenic medium, divided into three groups (control, PLA, and PLA/HA) at specific points (days 1, 3, and 7; three auxiliary wells at each time point). RNA concentration and purity were detected by Nanodrop 2000 after total RNA extraction. cDNA was acquired via extracted RNA reverse transcription process. Subsequently, the osteogenic differentiation potential of USCs on scaffolds was detected by real-time PCR (*OCN*, *COLI*, *ALP*, and *Runx2*). (Primer sequences are shown in Table 1).

Table 1
The sequence of analyzed gene primer for real-time PCR.

Gene	Primer
COL I	Forward: 5’-GGCCCTCAAGGTTTCCAAGG-3’
	Reverse: 5’-GGCCCTCAAGGTTTCCAAGG-3’
Runx2	Forward: 5’-CGTTCACTCCCATGACAAACA-3’
	Reverse: 5’-CGTTCACTCCCATGACAAACA-3’
OCN	Forward: 5’-CCCTGCACCTCATCCCTGA-3’
	Reverse: 5’-CCCTGCACCTCATCCCTGA-3’
ALP	Forward: 5’-GGCCTGTACCATACAAGCCC-3’
	Reverse: 5’-CCACGTAGACGAGGTAGTTGTG-3’

Rat cranial defect model

Eighteen Sprague–Dawley rats (no gender limitation, aged 6–8 weeks, average body weight 300 g) were anesthetized by intraperitoneal injection of 10% chloral hydrate. Circular defects of 5-mm diameter were drilled on both sides of the sagittal line with an orthopedic ring drill. Buprenorphine (0.05 mg/kg) was intraperitoneally injected for analgesia, and 200,000 U penicillin was intramuscularly injected for anti-inflammatory activity. A total of 36 skull defect models in 18 rats were randomly divided into the control group (n=12, without any treatment for the defect); PLA group (n=12, the defect area was implanted with PLA scaffold combined with USCs); and PLA/HA group (n=12, the defect area was implanted with PLA/HA scaffold combined with USCs).

Micro-CT, hematoxylin–eosin (HE) and Masson staining, and histological analysis

Six rats were killed at different intervals (4, 8, and 12 weeks) after treatment, and their skulls were removed to observe bone regeneration in the defect area. Samples were imaged with micro-CT with a resolution of 21 μm for scanning and imaging. 3D images of samples were obtained, and the data of newly formed bone area was calculated by Image J software (version 1.51k, NIH, USA) at each time point.

After being fixed in 4% paraformaldehyde solution, samples from different groups were washed and then placed in a 37℃ water bath for 7 days to remove calcium. Subsequently, the samples were embedded in paraffin and sliced into 5-μm thick sections. Histological analysis was performed by using HE staining. Masson staining showed the formation of fibers in the newly formed tissue. Besides, the tissue sections were immunohistochemically stained (*COLI* and *OCN)*. Final results were obtained using a fluorescence microscope.

Statistical analysis

GraphPad Prism (8.4.3) was used for statistical analysis of all experimental data. The statistical description method of quantitative data was mean ± SD, and ANOVA was used to analyze the differences between groups. $P < 0.05$ was considered to be statistically significant, and $P < 0.01$ was highly significant.

Results

Biological properties of USCs

USC colonies were visible under an optical microscope after 2 weeks of subculture (Fig. 1A). The morphology of the fourth-generation USCs showed slender shape, and some polygonal shapes (Fig. 1B). Flow cytometry analysis showed that surface antigens of blood cells (CD34, CD45, and MHC II HLA-DR) were not expressed or at a low level in USCs, while surface antigens of stem cells (CD73, CD90, and CD105) among over 95% of the USCs were highly expressed (Fig. 1C), which was consistent with previous research [28]. These observations suggest that USCs can be effectively isolated from the urine of healthy adults by the isolation culture method adopted in this study.

Alizarin red staining showed that the appearance of USCs changed to polygonal, and the number of red-stained calcium nodules in the cell mass increased (Fig. 2A). Alkaline phosphatase staining also indicated the formation of osteoblasts, which confirmed the osteogenic differentiation potential of USCs (Fig. 2B). Oil red O lipid staining suggested that the volume and nucleus of USCs were significantly increased after adipogenic induction, and a large number of red-stained lipid droplets were formed in the cytoplasm (Fig. 2C). The consequence of alcian blue staining showed that numerous mucopolysaccharides appeared in the microscopic field, which proved that USCs possess chondrogenic ability (Fig. 2D). Stem cells equipped with the potential ability of multidirectional differentiation and reproductive activity are quality seed cells that meet the requirements of bone tissue engineering. The characteristics of USCs determine their excellent performance in bone defect repair.

Characterization of 3D-printed scaffolds

The printed scaffolds appeared as a cube of 20·20·1.5 mm, and the pore size of the two scaffolds was between 300 and 500 um. The PLA scaffold was almost transparent (Fig. 3A), while the PLA/HA composite scaffold showed yellow (Fig. 3B). SEM revealed that these two kinds of scaffolds were neatly and evenly arranged, and pores were connected to each other (Fig. 3C, D). The vast surface area was conducive to the adhesion and growth of USCs. Besides, the total porosity of these scaffolds was more than 60% vol, which provided a necessary environment and ensured the conduction of nourishing substances for cell growth and the removal of metabolic waste (Fig. 3E). The degradation curves of these two kinds of scaffolds (Fig. 3F) suggested that the degradation speed of the PLA/HA scaffold was faster than that of the PLA scaffold. At 8 weeks after treatment, the degradation rates of PLA and PLA/HA scaffolds were 49.0%±0.7% and 53.6%±2.2%, respectively ($P \geq 0.05$).

In the case of EDS results, except for three elements (C/H/O), the PLA/HA composite scaffold also contained Ca and P, which confirmed the chemical component of HA, indicating that this kind of scaffold was a combination of PLA and HA (Fig. 3G, H).

As expected, the mechanical properties of the PLA scaffold were significantly improved after the addition of HA (Table 2). The Young's modulus of the PLA/HA scaffold (169.45±30.46 MPa) was nearly double that of the PLA scaffold (84.62±12.45 MPa). The ultimate deformation strength of PLA/HA scaffold (2.51±0.21) was approximately 1.5 times that of the PLA scaffold (1.65±0.19MPa). The results indicated that the biomechanical force of the pure PLA scaffold was enhanced with the addition of HA ($P<0.05$).

Table 2
Tested values of Young's modulus and ultimate deformation strength of PLA and PLA/HA scaffolds

samples	Young's modulus (MPa)	Ultimate deformation strength (MPa)
Cancellous Bone	425.19	75
PLA	84.62±12.45	1.65±0.19
PLA/HA	169.45±30.46	2.51±0.21

Cytocompatibility of printed scaffolds

After being cultivated for 3 days on scaffolds, USCs attached to the PLA scaffold and showed typical fibrous cell morphology, but only a small number of USCs could be found under SEM (Fig. 4A). However, in the PLA/HA group, as seen from the enlarged image, groups of USCs stretched out numerous filopodia and adhered tightly to the scaffold (Fig. 4B). Confocal microscopy showed that numerous filopodia around the surface of USCs clung to the scaffold. On the PLA/HA composite scaffold, the cytoskeleton of USCs was crosslinked into a network and spread evenly (Fig. 4D). However, on the PLA scaffold alone, USCs distributed over the whole surface unequally, and there were overlaps in the inner structure (Fig. 4C), which indicated that the PLA/HA composite scaffold may be more favorable for cell attachment and migration than the PLA scaffold alone. After being cultured with the leaching solution of different scaffolds, the CCK-8 assay showed that the cell growth curve in the scaffolds leaching solution was similar to that of the growth medium group at each time point ($P>0.05$) (Fig. 4E, F), indicating that cell proliferation was not affected, and the scaffolds had no toxic effect on USCs.

Expression of osteogenic genes of USCs on scaffolds

The expression of osteogenic genes (*OCN*, *COLI*, *ALP*, *Runx2*), which reveals bone remodeling, was detected by real-time quantitative PCR. The mRNA expression levels of *COLI*, *Runx2*, and *OCN* in the PLA and PLA/HA groups were significantly higher than those in the control group (Fig. 5A–D). The expression levels of *COLI*, *Runx2*, *OCN*, and *ALP* in the PLA/HA group were higher than those in the PLA group. However, the expression of *ALP* in the PLA group was lower than that in the control group.

Evaluation of repair of skull defect in rats

Bone defect repair was performed in each group and observed at 4, 8, and 12 weeks (Fig. 6). Bone regeneration in the samples receiving the scaffold treatment was significantly more effective than in the control group. Over time, the outlines of the scaffolds were vaguely visible, the boundaries between scaffolds and defect edge were blurred, and the newly formed bone was accumulated in the defect area. Bone defect repair in the PLA/HA group was more evident than in the PLA-only group. However, the PLA/HA composite scaffold with USCs promoted bone regeneration effectively.

Micro-CT images supported the general observations. Twelve weeks after treatment, there was little newly formed bone in the control group, with a bone formation of only 29.0%±0.9%, while PLA and PLA/HA groups showed a progressive amount of newly formed bone, starting from the border of the defect area and scaffolds, without any inflammation appeared in the area of implantation of USCs-seeded scaffolds (Fig. 7A). Radiographic images of the newly formed bone area of the regeneration process of PLA and PLA/HA scaffolds seeded with USCs indicated higher coverage of bone defect than in the control group (96.7%±1.6% vs 74.6%±1.9%, respectively), at 12 weeks after treatment (Fig. 7B). The difference was significant ($P<0.01$).

HE and Masson staining at 4, 8 and, 12 weeks after surgery showed similar tissue reaction among all the groups throughout the study (Fig. 8A, B). Four weeks after surgery, compared with the implantation group, only a few collagen fibers formed in the control group. However, a large number of collagen fibers were visible in the PLA and PLA/HA groups. The skull defect was filled with different amounts of new bone, with the shape of the scaffold visible. At 8 and 12 weeks after surgery, a large number of collagen fibers was observed in the control group, but only a small amount of new bone formed at the defect edge. In the PLA and PLA/HA groups, new bone tissue was formed progressively. Furthermore, in the PLA/HA group, the defect was filled with new bone, with only a small amount of scaffold material remaining in comparison with the PLA group. All these results indicate that PLA/HA can act as an adequate bone substitute and promote bone regeneration in the defect area.

Histological sections were observed with immunohistochemical staining of osteoblast markers at 12 weeks after treatment (*COLI* and *OCN*) to further assess osteogenic induction. *COLI* was positively expressed in the defect area in both PLA and PLA/HA groups (Fig. 9). Expression of *OCN* was evident in the newly formed bone tissue around the scaffold. At the same time, it was barely found in the control group. These results revealed that PLA/HA scaffolds with USCs significantly promoted osteogenic induction in the defect area.

Discussion

Bone defects have become common in clinical practice, while the natural healing process is challenging because of the poor regenerative capacity and large defects. In this study, the 3D-printed PLA/HA composite scaffold containing USCs was successfully applied to a rat model of skull defect. The PLA/HA scaffold has the advantage of two kinds of scaffold. The mechanical property of the PLA/HA scaffold increased and the degradation rate improved, while the inflammatory reaction in the defect area decreased. Besides, the feasibility of combining scaffolds with USCs was proved via the *in vitro* experiment. At 12 weeks after treatment, effective bone regeneration indicated the good therapeutic effect of PLA/HA scaffold and USCs in tissue engineering.

Applying bone tissue engineering technology in the treatment of bone defects, such as preparing 3D-printed scaffolds carrying seed cells, has been considered as a new treatment in recent years [16]. In a study about treatment outcomes of custom-made bioceramic implants, Staffa et al. [29] found that most

patients recovered well after surgery with few adverse consequences, which proved the osteogenic property of HA. It has also been found that the mechanical properties of HA are not strong enough to be used in large-scale defects [30]. Nevertheless, a single material does not have all the properties that tissue engineering requires. Therefore, different biopolymers and minerals were used to fabricate scaffolds with different properties [31]. Zimina et al. produced PLA/HA composites and showed their potential for hard tissue engineering and restoring maxillofacial defects [22]. Ideal scaffold materials in bone tissue engineering have higher biocompatibility, biodegradation, and mechanical strength; it is hard to achieve the purpose of bone defect repair otherwise [32, 33]. Although PLA has good biocompatibility and degradation ability, it is still deficient in mechanical strength and bone conductivity. Therefore, HA was combined with PLA in this study, and the results further proved that the mechanical performance and properties of composite scaffolds are superior to those of the materials acting independently (Table 2).

By extruding thermoplastic materials through a heated metal nozzle, the FDM fabrication produces various 3D designs [34]. For example, FDM-technology-printed porous polycaprolactone and hydroxyapatite (PCL/HA) scaffolds support cell adhesion and proliferation and relieve the adverse effects of inflammation on murine chondrocytes [35]. The physicochemical properties of the scaffold are crucial for the growth and differentiation of stem cells. It is believed that high porosity and interconnected pore structure of scaffolds are fundamental for bone regeneration in tissue engineering, and the optimum pore size ranges from 20 to 1500 μm. The size of the macropores of the scaffold is supposed to be >350 μm because seed cells need to migrate to the defect site and achieve bone regeneration [30]. Different pore sizes of scaffolds can be easily acquired by changing printing parameters like nozzle diameter, moving speed, and extrusion pressure [36]. In our study, PLA/HA composite scaffold was fabricated by FDM technology with the pore size ranging from 300 to 500 μm. The distribution and adhesion behavior of USCs in the PLA/HA group is more remarkable than that in other groups. We assume that the degradation component of PLA may reduce the pH in the environment, while alkaline HA has a buffering effect on acidic substances and provides suitable cell adhesion and proliferation conditions. Our results found that the PLA/HA composite scaffold showed better mechanical properties and cytocompatibility compared with the PLA-only scaffold (Fig. 4), in agreement with previous studies [22].

It seems possible to increase the mechanical properties of scaffolds by combining PLA with HA. However, we have to admit that even the maximum values of the Young's modulus and the ultimate deformation strength for the printed scaffolds are many times less than that of bone tissue; hence, it may be that printed scaffolds are not suitable for weight bearing. In our study, printed scaffolds were not used as load-bearing materials but for a sort of osteoinductive biomaterial containing USCs to promote bone regeneration in the defect site. In previous studies, biomaterials of scaffolds have played a crucial role in promoting bone regeneration. For instance, PLA/HA implantation in mice demonstrated good tolerance and widespread ingrowth of newly formed bone tissue into the implant pores [22]. Our *in vitro* results suggested that PLA/HA composite scaffolds induced a pronounced osteogenic gene expression (Fig. 5), which indicated that the PLA/HA composite scaffold enhanced the osteogenic potential of USCs.

Although different materials exhibit their ability to repair bone defects, successful bone regeneration still requires seed cells, which can differentiate into other types of cells. Seed cells have long been seeded onto scaffolds for tissue engineering, such as bone marrow MSCs, adipose-derived stem cells, muscle-derived stem cells, and embryonic stem cells [37–40]. However, the clinical application of most seed cells was limited by various factors such as limited sampling sites, insufficient donors, and ill-equipped cell homing. Similar to other adult stem cells, USCs conform to seed cells' characteristics in terms of growth pattern and differentiation capacity, and it have been successfully used for urinary system, nerve tissue, and skeletal muscle tissue injury [11–14]. Our work showed that USCs expressed the surface marker of bone marrow MSCs, with conspicuous cell proliferation ability and multiple differentiation potential (Fig. 1). Besides, USCs have been used for the repair and reconstruction of bone defects. For example, the combination of PLGA/CS scaffolds and USCs has potential in bone regeneration since they can stimulate osteogenic differentiation of USCs and induce ingrowth of blood vessels into scaffolds [41]. Many researchers have attempted to find methods to induce USCs into the osteogenic lineage [42], whereas few studies have focused on combining USCs with scaffolds suitable for tissue engineering. Furthermore, the effects of PLA/HA composite scaffolds on osteogenic differentiation of USCs have not been reported. So, we fabricated the PLA/HA composite scaffold via FDM 3D printing technology. USCs were inoculated onto scaffolds, which were subsequently transplanted into rats to analyze the osteogenic differentiation of USCs.

Our *in vivo* study showed that PLA/HA scaffold containing USCs repaired bone defects at the macro- and micro-level (Figs. 6–8). Whether in the results of the general observation or micro-CT images, the implantation group showed a better therapeutic effect than the control group at 12 weeks after treatment. The dimension of newly formed bone by micro-CT analysis indicated that the PLA/HA scaffolds containing USCs had the best performance in reconstructing bone defects and the fastest rate of scaffold degradation. Osteocalcin (*OCN*) is a biochemical marker that is produced by osteoblasts. It plays a vital role in bone-building and late osteogenesis. Compared with other groups, more *OCN* was expressed in PLA/HA groups, indicating that the PLA/HA scaffold further promoted osteogenic differentiation of USCs. The PLA/HA scaffold containing USCs caused more marked bone regeneration in the skull defect model than the PLA scaffold with USCs.

There were several limitations to our work. Although USCs have been successfully seeded onto PLA/HA scaffolds and applied to bone defect repair, it is still unclear whether USCs can be widely applied to other kinds of scaffolds. Also, we evaluated bone defect repair, but the weight-bearing capacity and mechanical properties of the newly formed bone in the defect area still have to be further tested. Finally, in this bone defect model, we did not analyze the mechanism of bone defect repair, which requires further investigation.

Conclusion

The PLA/HA composite scaffold prepared by 3D printing has excellent biocompatibility and mechanical intensity. *In vivo* test results demonstrate that the PLA/HA scaffold containing USCs can promote

progressive regeneration of bone tissues in the defect area. These findings support that composite scaffold inoculated with USCs is a reliable solution for bone tissue engineering.

Abbreviations

PLA: Polylactic acid

HA: Hydroxyapatite

USCS: Urine-derived stem cells

3D: Three-dimensional

CAD: Computer-aided design

FDM: Fused-deposition modeling

PBS: Phosphate buffered saline

FBS: Fetal bovine serum

PDGF: Platelet-derived growth factor

TGF-b: Transforming growth factor-b

DMEM: Dulbecco's modified eagle medium

EDS: Energy-dispersive X-ray spectroscopy

SEM: Scanning electron microscopy

IACUC: Institutional Animal Care and Use Committee

Declarations

Ethics approval

All the animal experiments were performed after receiving the approval of the Institutional Animal Care and Use Committee (IACUC) in Sichuan University, Chengdu, Sichuan Province, China (No.2020072A).

Consent for publication

Not applicable.

Availability of data and materials

The datasets used and/or analyzed during the current study are available from the corresponding author on reasonable request.

Competing interests

The authors declared that they have no competing interests.

Funding

This work was supported by the National Natural Science Foundation of China (31870961, 81501879), the Sino-German Center for Research Promotion (GZ1219), and the International Cooperation Project of the Science and Technology Department of Sichuan Province (Grant No. 2015HH0049, No. 2017SZ0127).

Authors' contributions

XZ and JLC contributed equally to this work. XZ and JLC designed the study and analyzed the study data and drafted the manuscript. HRW and FG corrected the study data and searched the relative literature. XD revised the manuscript and supervised the study. All authors read and approved the final manuscript.

Acknowledgements

Not applicable.

Authors' information

[1]Department of Orthopedics, West China Hospital, Sichuan University, Chengdu, China. [2]Department of Pathogen Biology, West China School of Basic Medical Sciences & Forensic Medicine, Sichuan University, Chengdu, China. [3]Department of Orthopedics, Ganzi Tibetan Autonomous Prefecture People's Hospital, Ganzi Prefecture, Sichuan Province, China

References

1. El-Rashidy AA, Roether JA, Harhaus L, Kneser U, Boccaccini AR. Regenerating bone with bioactive glass scaffolds: A review of in vivo studies in bone defect models. Acta Biomater. 2017;62:1–28.
2. Garcia-Gareta E, Coathup MJ, Blunn GW. Osteoinduction of bone grafting materials for bone repair and regeneration. Bone. 2015;81:112–21.

3. Trauner KB. The Emerging Role of 3D Printing in Arthroplasty and Orthopedics. The Journal of Arthroplasty. 2018;33(8):2352–4.
4. Swetha S, Lavanya K, Sruthi R, Selvamurugan N. An insight into cell-laden 3D-printed constructs for bone tissue engineering. Journal of materials chemistry B. 2020;8(43):9836–62.
5. Chamberlain JR, Schwarze U, Wang PR, Hirata RK, Hankenson KD, Pace JM, Underwood RA, Song KM, Sussman M, Byers PH, et al. Gene targeting in stem cells from individuals with osteogenesis imperfecta. Science. 2004;303(5661):1198–201.
6. Dominici M, Le Blanc K, Mueller I, Slaper-Cortenbach I, Marini F, Krause D, Deans R, Keating A, Prockop D, Horwitz E. Minimal criteria for defining multipotent mesenchymal stromal cells. The International Society for Cellular Therapy position statement. Cytotherapy. 2006;8(4):315–7.
7. Zhang D, Wei G, Li P, Zhou X, Zhang Y. Urine-derived stem cells: A novel and versatile progenitor source for cell-based therapy and regenerative medicine. Genes diseases. 2014;1(1):8–17.
8. Qin H, Zhu C, An Z, Jiang Y, Zhao Y, Wang J, Liu X, Hui B, Zhang X, Wang Y. Silver nanoparticles promote osteogenic differentiation of human urine-derived stem cells at noncytotoxic concentrations. Int J Nanomed. 2014;9:2469–78.
9. Burdeyron P, Giraud S, Hauet T, Steichen C. Urine-derived stem/progenitor cells: A focus on their characterization and potential. World journal of stem cells. 2020;12(10):1080–96.
10. Bodin A, Bharadwaj S, Wu S, Gatenholm P, Atala A, Zhang Y. Tissue-engineered conduit using urine-derived stem cells seeded bacterial cellulose polymer in urinary reconstruction and diversion. Biomaterials. 2010;31(34):8889–901.
11. Liu Y, Ma W, Liu B, Wang Y, Chu J, Xiong G, Shen L, Long C, Lin T, He D, et al. Urethral reconstruction with autologous urine-derived stem cells seeded in three-dimensional porous small intestinal submucosa in a rabbit model. Stem Cell Res Ther. 2017;8(1):63.
12. Zhang C, George SK, Wu R, Thakker PU, Abolbashari M, Kim TH, Ko IK, Zhang Y, Sun Y, Jackson J, et al. Reno-protection of Urine-derived Stem Cells in A Chronic Kidney Disease Rat Model Induced by Renal Ischemia and Nephrotoxicity. Int J Biol Sci. 2020;16(3):435–46.
13. Ling X, Zhang G, Xia Y, Zhu Q, Zhang J, Li Q, Niu X, Hu G, Yang Y, Wang Y, et al. Exosomes from human urine-derived stem cells enhanced neurogenesis via miR-26a/HDAC6 axis after ischaemic stroke. J Cell Mol Med. 2020;24(1):640–54.
14. Wu R, Huang C, Wu Q, Jia X, Liu M, Xue Z, Qiu Y, Niu X, Wang Y. Exosomes secreted by urine-derived stem cells improve stress urinary incontinence by promoting repair of pubococcygeus muscle injury in rats. Stem Cell Res Ther. 2019;10(1):80.
15. Mironov V, Boland T, Trusk T, Forgacs G, Markwald RR. Organ printing: computer-aided jet-based 3D tissue engineering. Trends Biotechnol. 2003;21(4):157–61.
16. Lin K, Sheikh R, Romanazzo S, Roohani I. 3D Printing of Bioceramic Scaffolds—Barriers to the Clinical Translation: From Promise to Reality, and Future Perspectives. Materials. 2019;12(17):2660.
17. Tagami T, Nagata N, Hayashi N, Ogawa E, Fukushige K, Sakai N, Ozeki T. Defined drug release from 3D-printed composite tablets consisting of drug-loaded polyvinylalcohol and a water-soluble or

water-insoluble polymer filler. International journal of pharmaceutics. 2018;543(1-2):361–7.

18. Garg B, Mehta N. Current status of 3D printing in spine surgery. Journal of clinical orthopaedics trauma. 2018;9(3):218–25.
19. Sridharan R, Cavanagh B, Cameron AR, Kelly DJ, O'Brien FJ. Material stiffness influences the polarization state, function and migration mode of macrophages. Acta biomaterialia. 2019;89:47–59.
20. Zhang H, Mao X, Du Z, Jiang W, Han X, Zhao D, Han D, Li Q. Three dimensional printed macroporous polylactic acid/hydroxyapatite composite scaffolds for promoting bone formation in a critical-size rat calvarial defect model. Sci Technol Adv Mater. 2016;17(1):136–48.
21. Zhang H, Mao X, Zhao D, Jiang W, Du Z, Li Q, Jiang C, Han D. Three dimensional printed polylactic acid-hydroxyapatite composite scaffolds for prefabricating vascularized tissue engineered bone: An in vivo bioreactor model. Scientific reports. 2017;7(1):15255.
22. Zimina A, Senatov F, Choudhary R, Kolesnikov E, Anisimova N. Biocompatibility and Physico-Chemical Properties of Highly Porous PLA/HA Scaffolds for Bone Reconstruction. 2020, 12(12).
23. Gao P, Han P, Jiang D, Yang S, Cui Q, Li Z. Effects of the donor age on proliferation, senescence and osteogenic capacity of human urine-derived stem cells. Cytotechnology. 2017;69(5):751–63.
24. Liu G, Pareta RA, Wu R, Shi Y, Zhou X, Liu H, Deng C, Sun X, Atala A, Opara EC, et al. Skeletal myogenic differentiation of urine-derived stem cells and angiogenesis using microbeads loaded with growth factors. Biomaterials. 2013;34(4):1311–26.
25. Alksne M, Kalvaityte M, Simoliunas E, Rinkunaite I, Gendviliene I, Locs J, Rutkunas V, Bukelskiene V. In vitro comparison of 3D printed polylactic acid/hydroxyapatite and polylactic acid/bioglass composite scaffolds: Insights into materials for bone regeneration. J Mech Behav Biomed Mater. 2020;104:103641.
26. Alksne M, Simoliunas E, Kalvaityte M, Skliutas E, Rinkunaite I, Gendviliene I, Baltriukiene D, Rutkunas V, Bukelskiene V. The effect of larger than cell diameter polylactic acid surface patterns on osteogenic differentiation of rat dental pulp stem cells. Journal of biomedical materials research Part A. 2019;107(1):174–86.
27. Qi C, Deng Y, Xu L, Yang C, Zhu Y, Wang G, Wang Z, Wang L. A sericin/ graphene oxide composite scaffold as a biomimetic extracellular matrix for structural and functional repair of calvarial bone. Theranostics. 2020;10(2):741–56.
28. Chen AJ, Pi JK, Hu JG, Huang YZ, Gao HW, Li SF, Li-Ling J, Xie HQ. Identification and characterization of two morphologically distinct stem cell subpopulations from human urine samples. Science China Life sciences. 2020;63(5):712–23.
29. Staffa G, Barbanera A, Faiola A, Fricia M, Limoni P, Mottaran R, Zanotti B, Stefini R. Custom made bioceramic implants in complex and large cranial reconstruction: a two-year follow-up. Journal of cranio-maxillo-facial surgery: official publication of the European Association for Cranio-Maxillo-Facial Surgery 2012, 40(3):e65-70.

30. Koupaei N, Karkhaneh A. Porous crosslinked polycaprolactone hydroxyapatite networks for bone tissue engineering. Tissue engineering regenerative medicine. 2016;13(3):251–60.
31. Houben A, Van Hoorick J, Van Erps J, Thienpont H, Van Vlierberghe S, Dubruel P. Indirect Rapid Prototyping: Opening Up Unprecedented Opportunities in Scaffold Design and Applications. Ann Biomed Eng. 2017;45(1):58–83.
32. Mondschein RJ, Kanitkar A, Williams CB, Verbridge SS, Long iE. Polymer structure-property requirements for stereolithographic 3D printing of soft tissue engineering scaffolds. Polymers 2017:170–188.
33. Sheikh Z, Hamdan N, Ikeda Y, Grynpas M, Ganss B, Glogauer M. Natural graft tissues and synthetic biomaterials for periodontal and alveolar bone reconstructive applications: a review. Biomaterials research. 2017;21:9.
34. Xu N, Ye X, Wei D, Zhong J, Chen Y, Xu G, He D. 3D artificial bones for bone repair prepared by computed tomography-guided fused deposition modeling for bone repair. ACS Appl Mater Interfaces. 2014;6(17):14952–63.
35. Gong L, Li J, Zhang J, Pan Z, Liu Y, Zhou F, Hong Y, Hu Y, Gu Y, Ouyang H, et al. An interleukin-4-loaded bi-layer 3D printed scaffold promotes osteochondral regeneration. Acta Biomater. 2020;117:246–60.
36. Olubamiji AD, Izadifar Z, Si JL, Cooper DM, Eames BF, Chen DX. Modulating mechanical behaviour of 3D-printed cartilage-mimetic PCL scaffolds: influence of molecular weight and pore geometry. Biofabrication. 2016;8(2):025020.
37. Yamaguchi Y, Ohno J, Sato A, Kido H, Fukushima T. Mesenchymal stem cell spheroids exhibit enhanced in-vitro and in-vivo osteoregenerative potential. BMC Biotechnol. 2014;14:105.
38. Riegger J, Palm HG, Brenner RE. The functional role of chondrogenic stem/progenitor cells: novel evidence for immunomodulatory properties and regenerative potential after cartilage injury. European cells materials. 2018;36:110–27.
39. Liu X, Wang P, Chen W, Weir MD, Bao C, Xu HH. Human embryonic stem cells and macroporous calcium phosphate construct for bone regeneration in cranial defects in rats. Acta Biomater. 2014;10(10):4484–93.
40. Mohamed-Ahmed S, Yassin MA, Rashad A, Espedal H, Idris SB, Finne-Wistrand A, Mustafa K, Vindenes H, Fristad I. Comparison of bone regenerative capacity of donor-matched human adipose-derived and bone marrow mesenchymal stem cells. Cell tissue research. 2021;383(3):1061–75.
41. Guan J, Zhang J, Guo S, Zhu H, Zhu Z, Li H, Wang Y, Zhang C, Chang J. Human urine-derived stem cells can be induced into osteogenic lineage by silicate bioceramics via activation of the Wnt/beta-catenin signaling pathway. Biomaterials. 2015;55:1–11.
42. Guan J, Zhang J, Zhu Z, Niu X, Guo S, Wang Y, Zhang C. Bone morphogenetic protein 2 gene transduction enhances the osteogenic potential of human urine-derived stem cells. Stem Cell Res Ther. 2015;6(1):5.

Figures

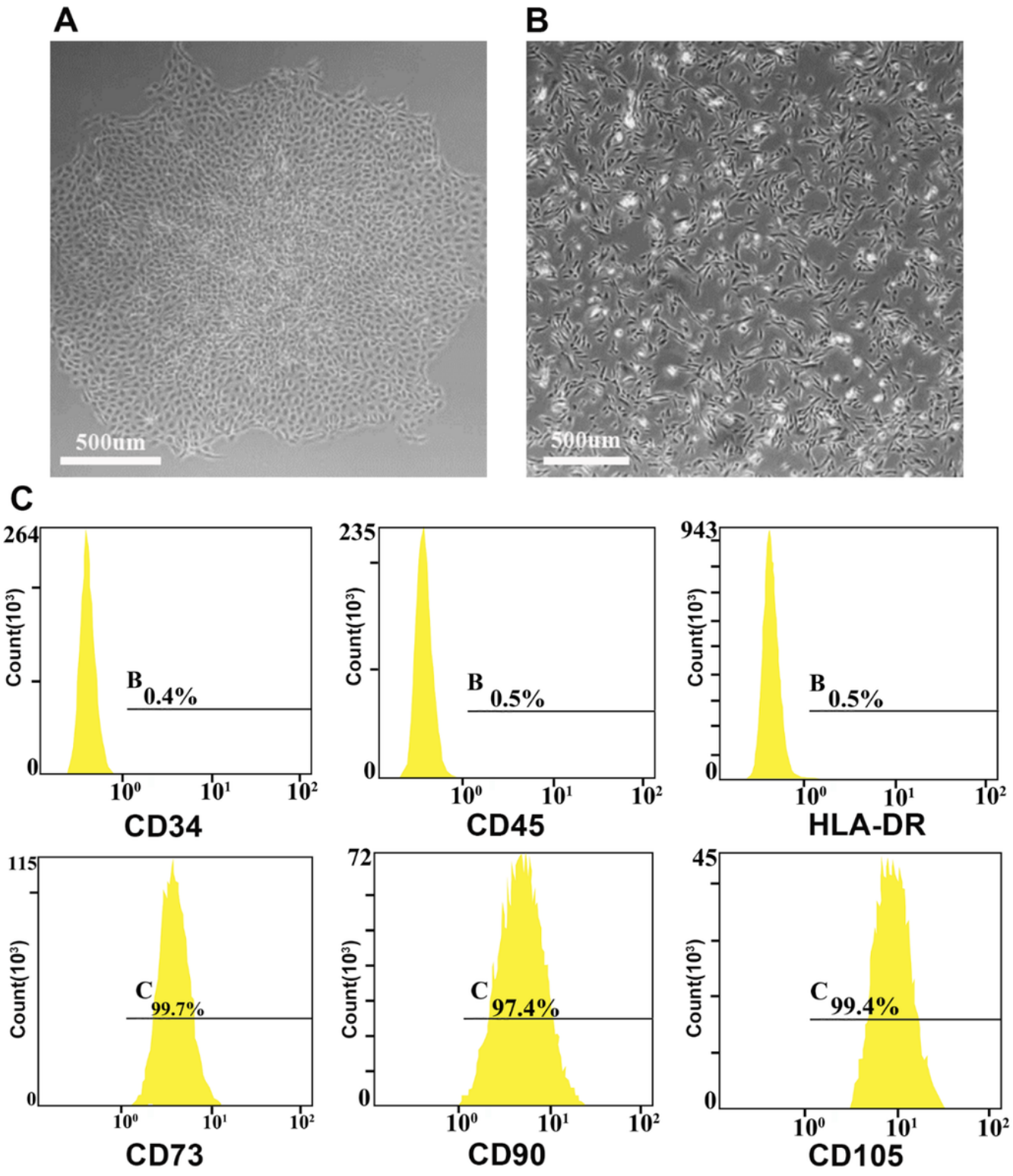

Figure 1

USCs identified with microscopy and flow cytometry; A Morphology of the cultured primary USCs for 2 weeks; B Morphology of the fourth generation USCs; C Flow cytometry results of cell surface negative (CD34, CS45, HLA-DR) and positive (CD73, CD90, CD105) antigens of the fourth generation USCs.

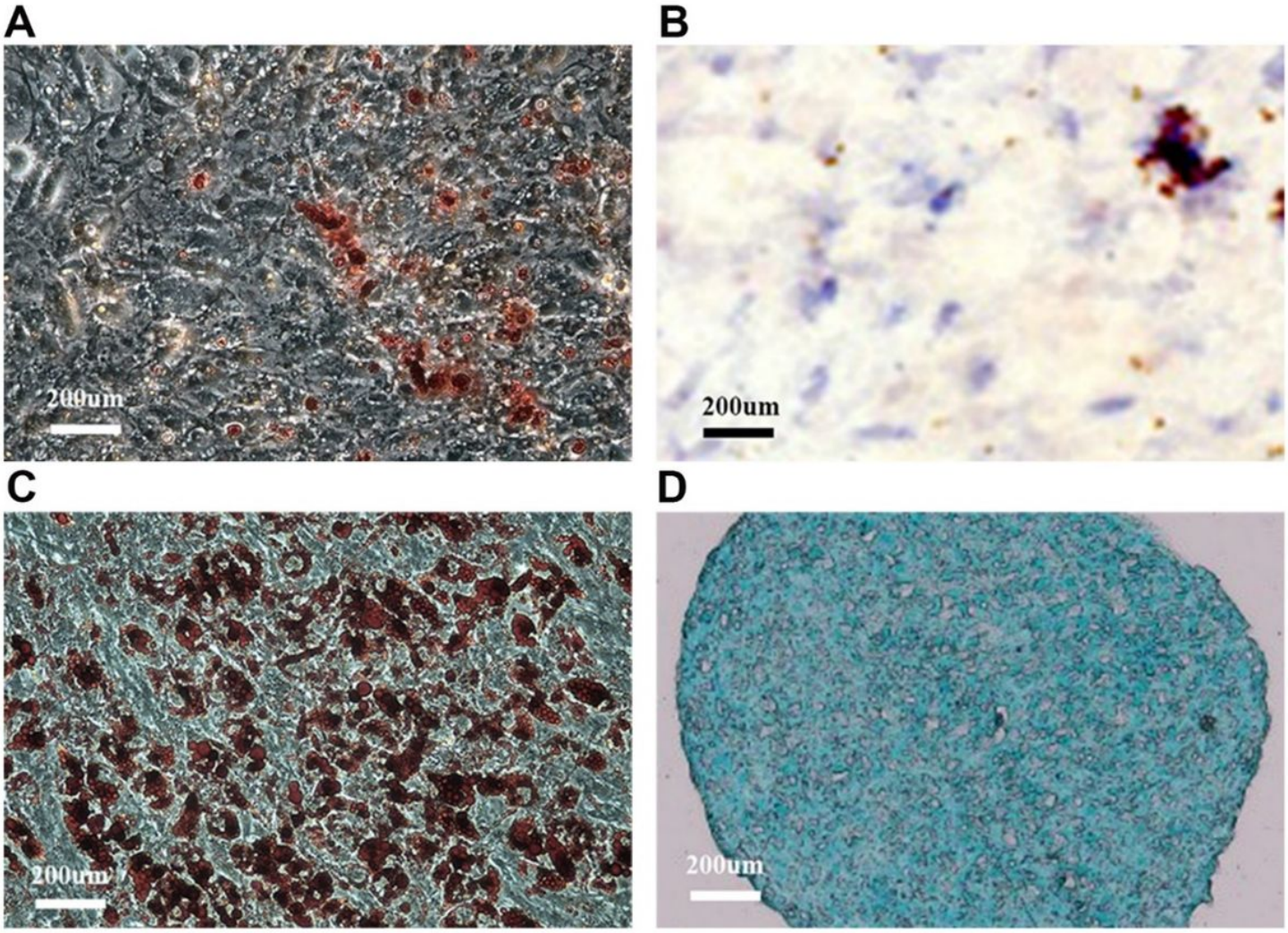

Figure 2

Differentiation results of USCs; A Alizarin red staining; B Alkaline phosphatase staining; C Oil red O lipid staining; D Alcian blue staining.

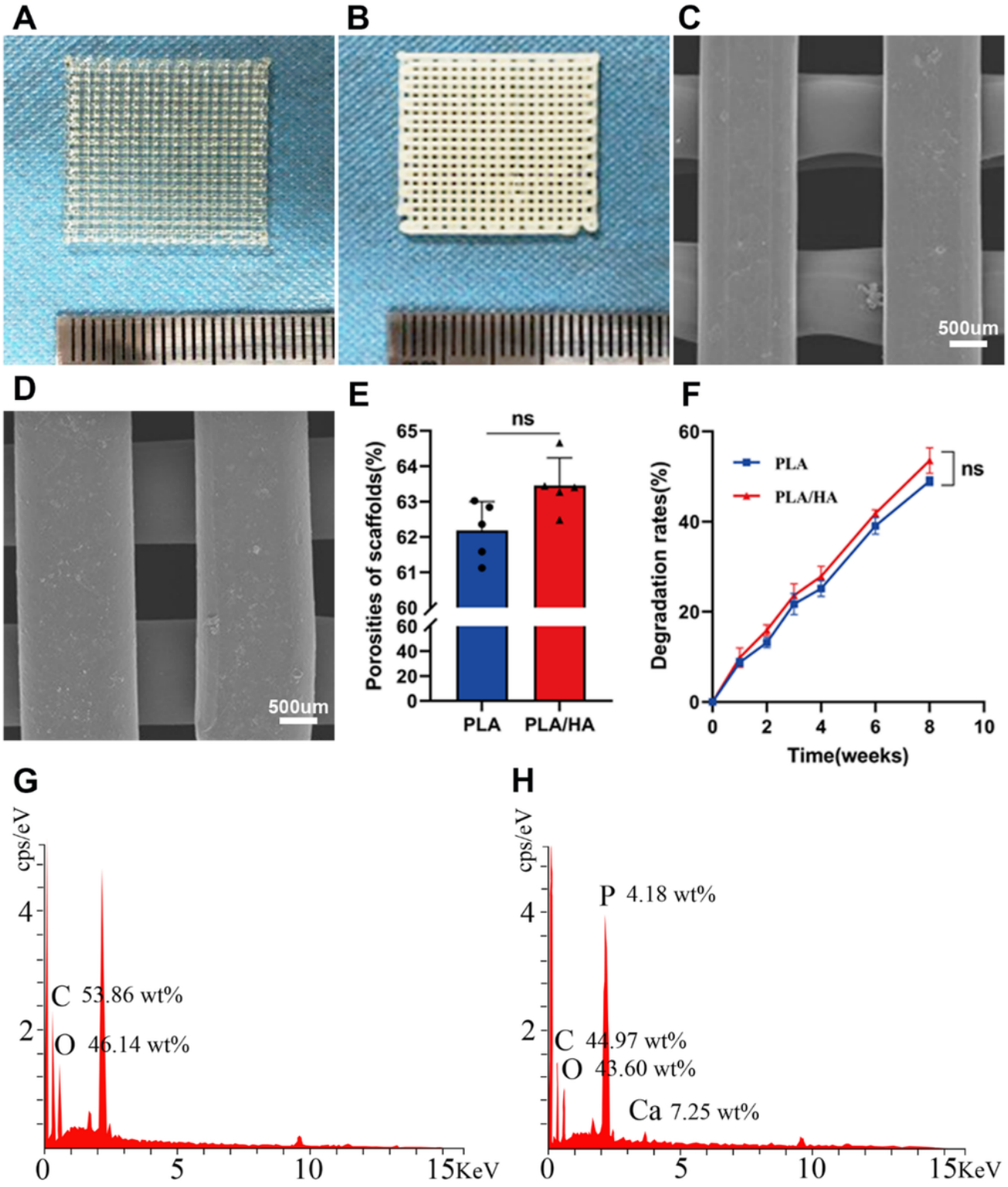

Figure 3

Preparation and characterization of the scaffolds; Overview of PLA (A) and PLA/HA (B) scaffolds; SEM images of PLA (C) and PLA/HA (D) scaffolds; The porosities (E) and degradation rates (F) of PLA and PLA/HA scaffolds; G, H Electron dispersive X-ray spectroscopy (EDS) analysis indicates Ca and P's presence in the PLA/HA scaffold.

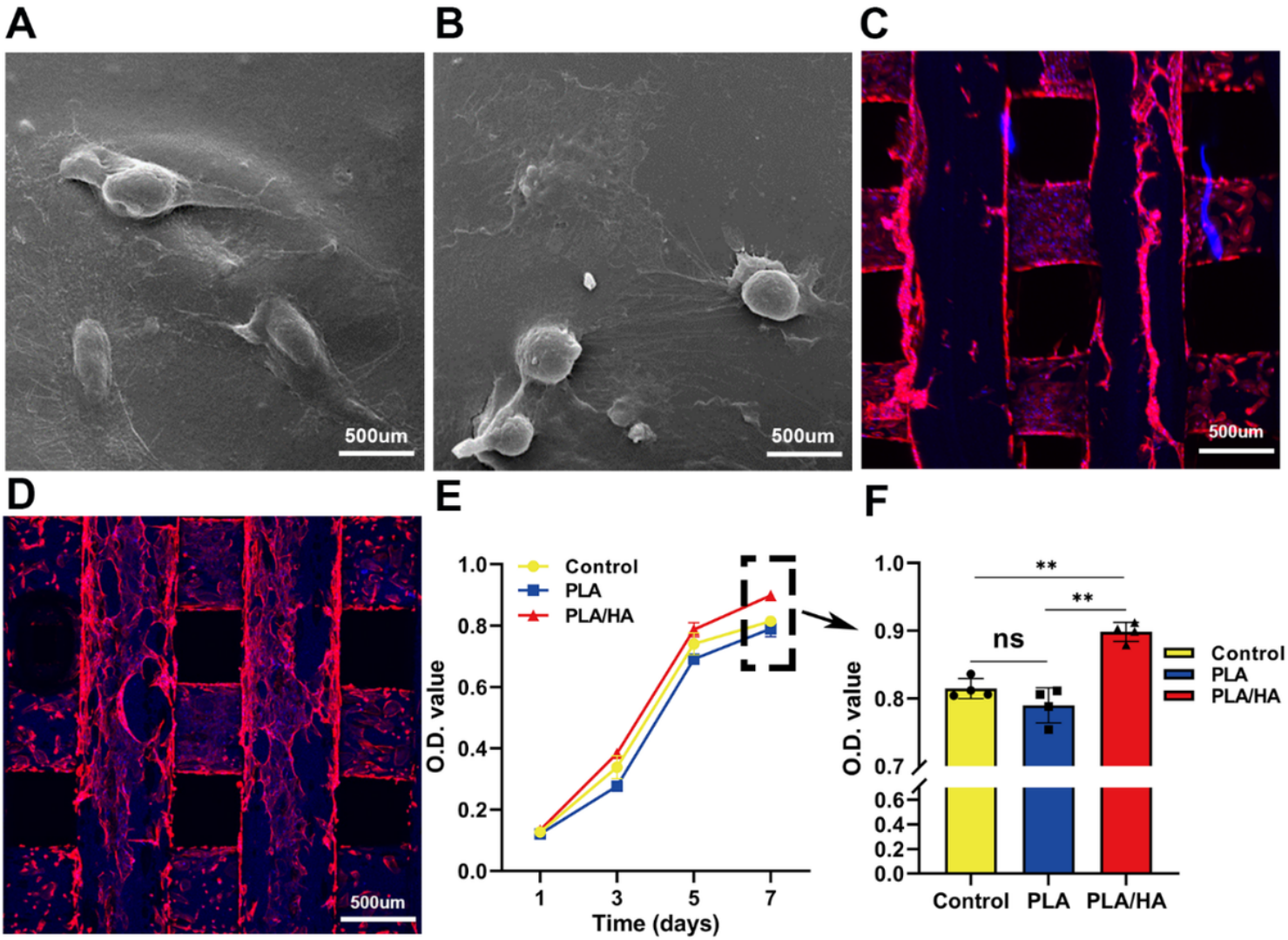

Figure 4

Cytocompatibility test of scaffolds; The electronic microscope scanning of USCs on PLA (A) and PLA/HA (B) scaffolds; Cytoskeleton investigated under laser confocal microscopy (C PLA scaffold; D PLA/HA scaffold); E, F The growth of USCs in control group and scaffolds leaching liquor groups at each time point (1, 3, 5, 7 days after experiment). *p < 0.05; **p < 0.01

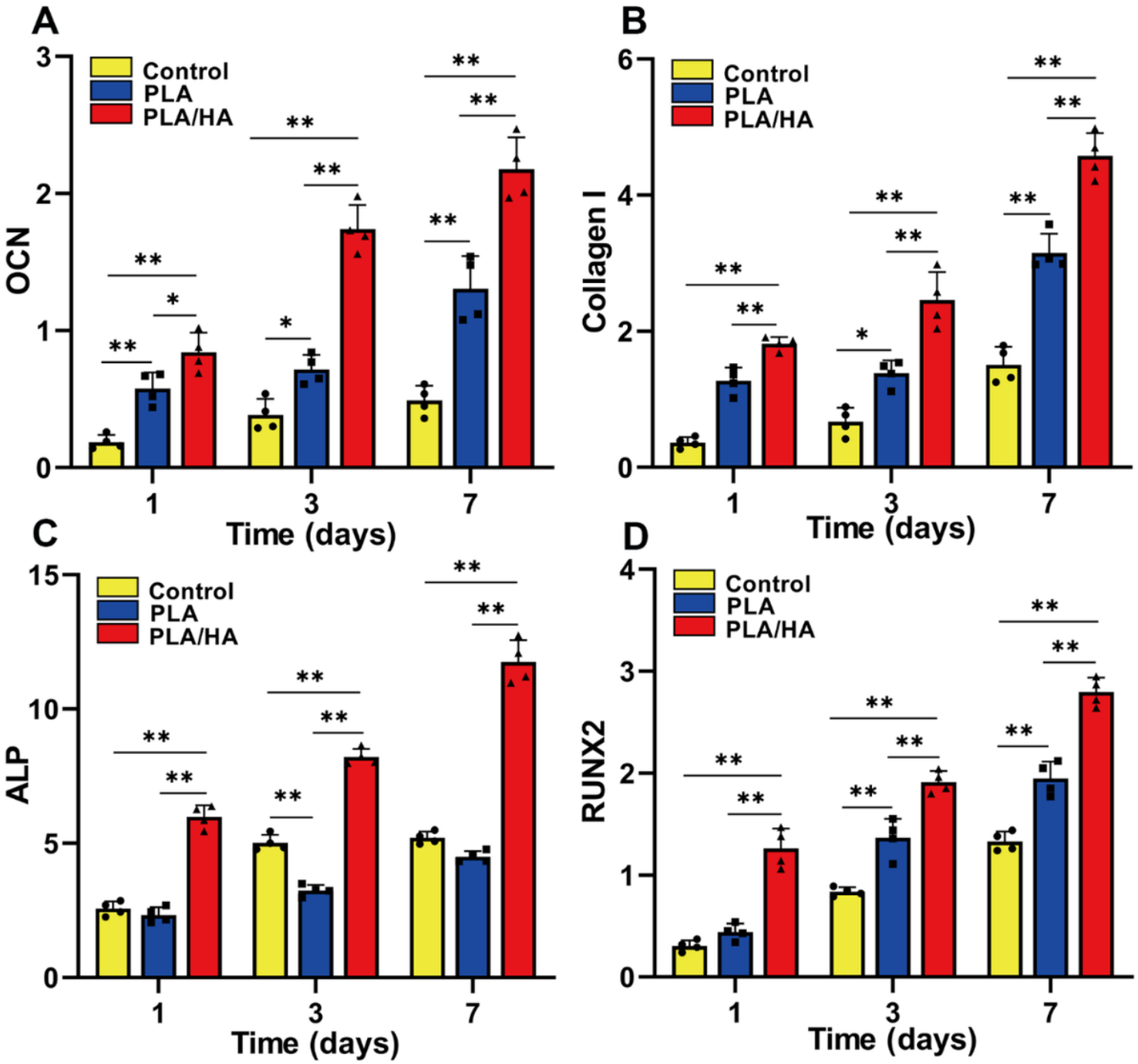

Figure 5

Relative quantitation of mRNA expression levels of osteogenic genes in different groups (Control, PLA and PLA/HA groups) at each time point (1, 3, 7 days after experiment); A OCN; B COL I; C ALP; D RUNX2. *p < 0.05; **p < 0.01

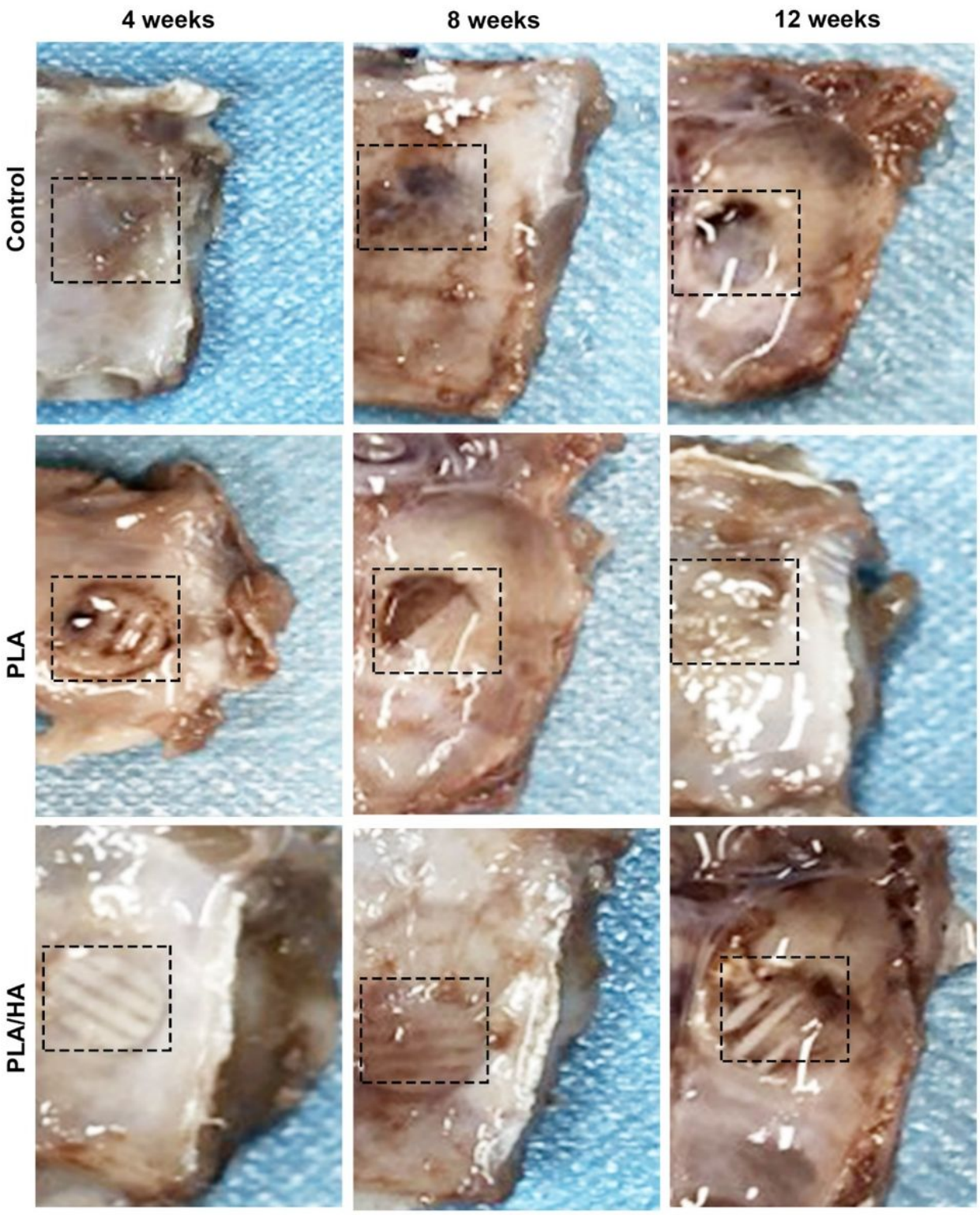

Figure 6

Photographs of the skull defects in rats receiving no treatment (control), PLA with USCs, and PLA/HA with USCs treatment at each time point (4, 8, and 12weeks after treatment).

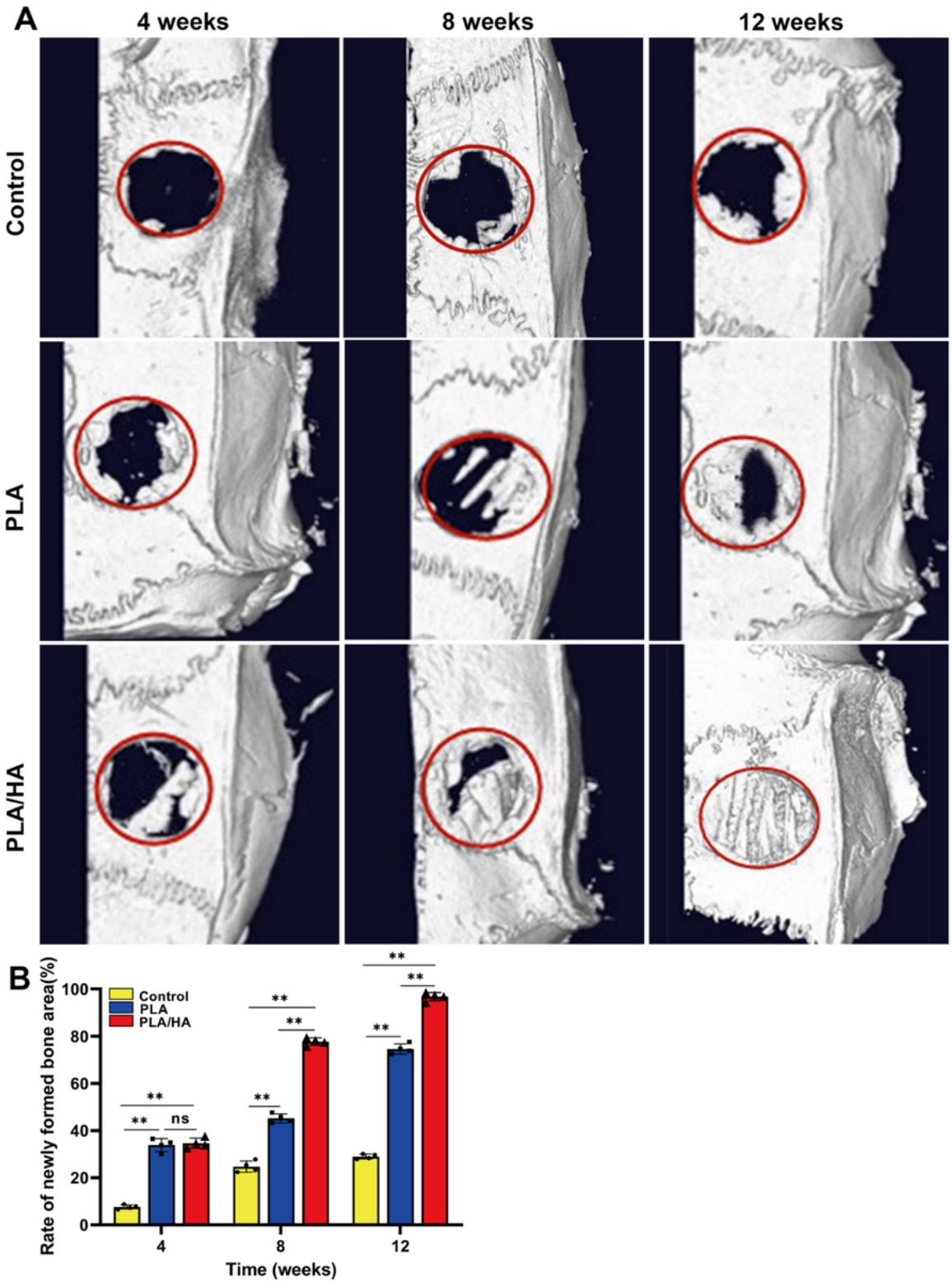

Figure 7

A Images reconstructed by micro-CT showed bone regeneration in different groups (control, PLA, and PLA/HA) at each time point (4, 8 and 12weeks after treatment); B The rate of newly formed bone tissue measured by Image J software (version 1.51k, NIH, USA). *p < 0.05; **p < 0.01

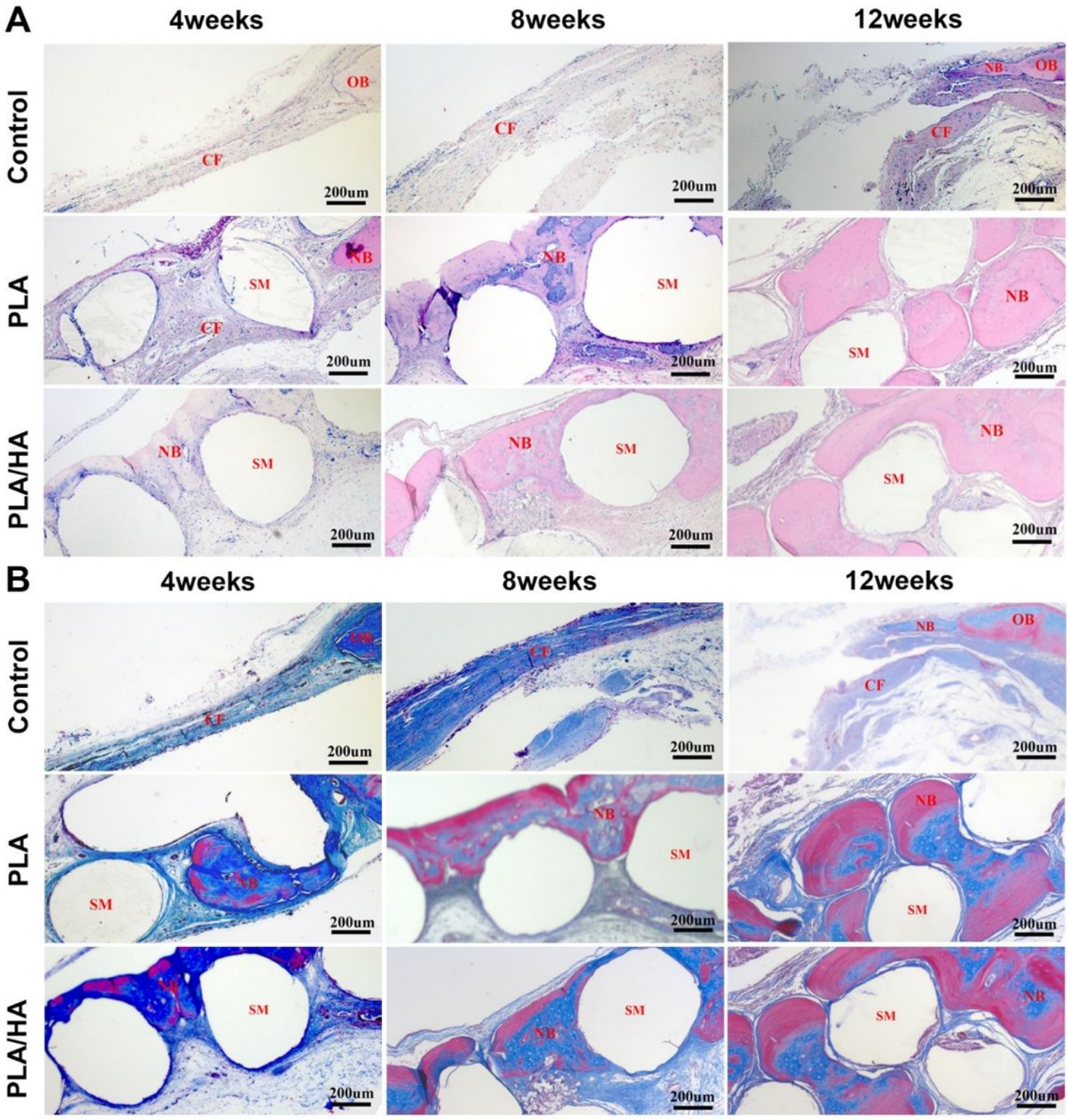

Figure 8

Immunohistochemical staining in different groups at 4, 8, and 12 weeks; A Hematoxylin-eosin (H&E) and B Masson's trichrome staining of tissue sections in different groups at 4, 8 and, 12 weeks after surgeon. OB: original bone tissue; CF: collagen fiber; SM: scaffold materials; NB: new bone tissue

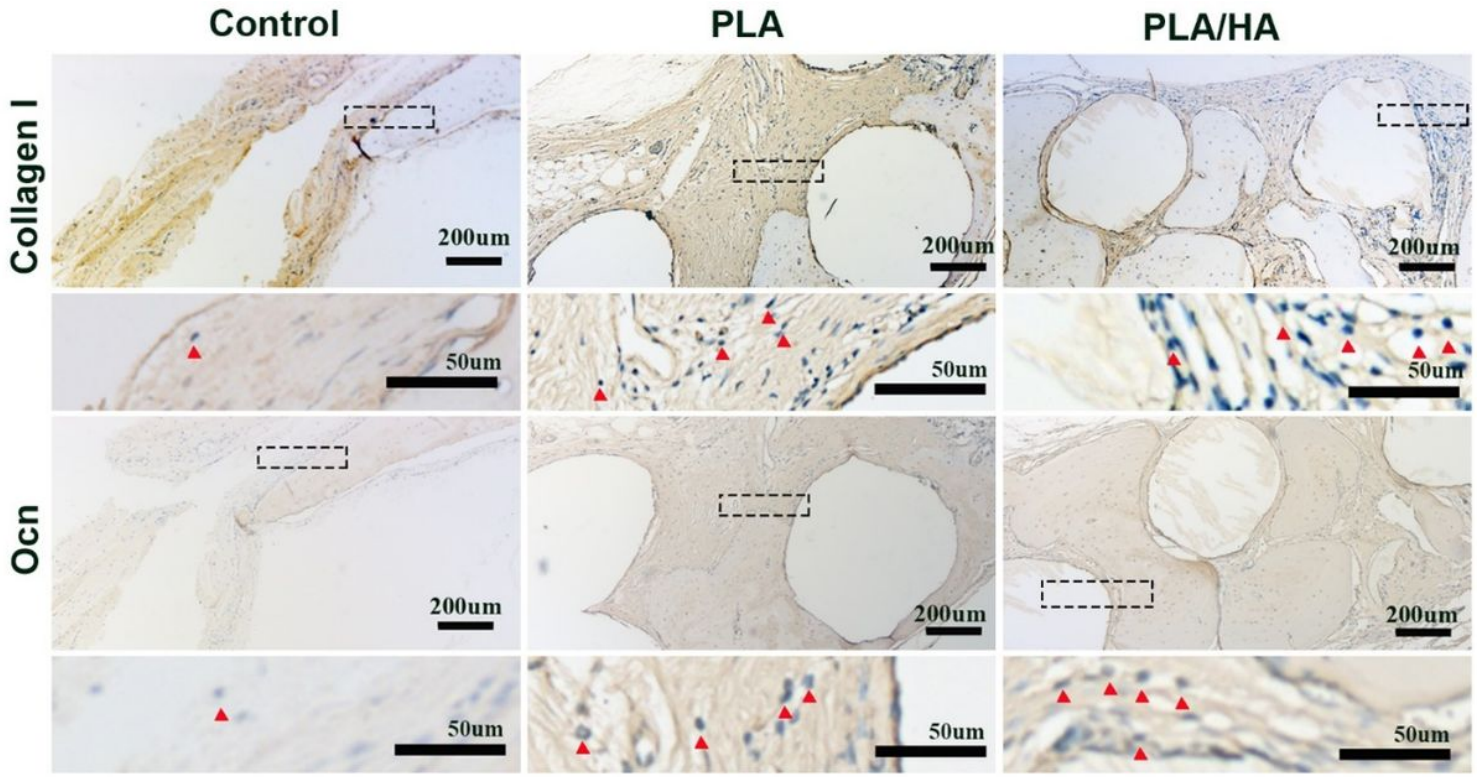

Figure 9

The immunohistochemical staining of Collagen I and OCN in different groups at 12 weeks.